

Radial wall strain: a novel angiographic measure of plaque composition and vulnerability

Huihong Hong^{1,2}, MD; Chunming Li², BSc; Juan Luis Gutiérrez-Chico³, MD, PhD; Zhiqing Wang¹, MD; Jiayue Huang⁴, MSc; Miao Chu², PhD; Takashi Kubo⁵, MD, PhD; Lianglong Chen^{1*}, MD, PhD; William Wijns⁴, MD, PhD; Shengxian Tu^{1,2*}, PhD

1. Department of Cardiology, Fujian Medical University Union Hospital, Fuzhou, China; 2. Biomedical Instrument Institute, School of Biomedical Engineering, Shanghai Jiao Tong University, Shanghai, China; 3. Department of Cardiology, Ruijin Hospital, Shanghai Jiao Tong University School of Medicine, Shanghai, China; 4. The Lambe Institute for Translational Medicine, The Smart Sensors Laboratory and Curam, National University of Ireland Galway, Galway, Ireland; 5. Department of Cardiovascular Medicine, Wakayama Medical University, Wakayama, Japan

H. Hong and C. Li contributed equally to this manuscript. L. Chen and S. Tu are joint corresponding authors.

This paper also includes supplementary data published online at: <https://eurointervention.pronline.com/doi/10.4244/EIJ-D-22-00537>

KEYWORDS

- optical coherence tomography
- plaque rupture
- QCA

Abstract

Background: The lipid-to-cap ratio (LCR) and thin-cap fibroatheroma (TCFA) derived from optical coherence tomography (OCT) are indicative of plaque vulnerability.

Aims: We aimed to explore the association of a novel method to estimate radial wall strain (RWS) from angiography with plaque composition and features of vulnerability assessed by OCT.

Methods: Anonymised data from patients with intermediate stenosis who underwent coronary angiography (CAG) and OCT were analysed in a core laboratory. Angiography-derived RWS_{max} was computed as the maximum deformation of lumen diameter throughout the cardiac cycle, expressed as a percentage of the largest lumen diameter. The LCR and TCFA were automatically determined on OCT images by a recently validated algorithm based on artificial intelligence.

Results: OCT and CAG images from 114 patients (124 vessels) were analysed. The average time for the analysis of RWS_{max} was 57 (39-82) seconds. The RWS_{max} in the interrogated plaques was 12% (10-15%) and correlated positively with the LCR ($r=0.584$; $p<0.001$) and lipidic plaque burden ($r=0.411$; $p<0.001$), and negatively with fibrous cap thickness ($r=-0.439$; $p<0.001$). An $RWS_{max}>12\%$ was an angiographic predictor for an LCR >0.33 (area under the curve [AUC]=0.86, 95% confidence interval [CI]: 0.78-0.91; $p<0.001$) and TCFA (AUC=0.72, 95% CI: 0.63-0.80; $p<0.001$). Lesions with $RWS_{max}>12\%$ had a higher prevalence of TCFA (22.0% versus 1.5%; $p<0.001$), thinner fibrous cap thickness (71 μm versus 101 μm ; $p<0.001$), larger lipidic plaque burden (23.3% versus 15.4%; $p<0.001$), and higher maximum LCR (0.41 versus 0.18; $p<0.001$) compared to lesions with $RWS_{max}\leq 12\%$.

Conclusions: Angiography-derived RWS was significantly correlated with plaque composition and known OCT features of plaque vulnerability in patients with intermediate coronary stenosis.

*Corresponding authors: Lianglong Chen, Department of Cardiology, Fujian Heart Medical Centre, Fujian Medical University Union Hospital, 29 Xin-Quan Rd, Fuzhou, Fujian, 350001, China. E-mail: lianglongchenfj@126.com
Shengxian Tu, Room 123, Med-X Research Institute, Shanghai Jiao Tong University, No. 1954 Hua Shan Road, Shanghai 200030, China. E-mail: sxtu@sjtu.edu.cn

Abbreviations

%DS	percent diameter stenosis
AI	artificial intelligence
CAD	coronary artery disease
CAG	coronary angiography
FCT	fibrous cap thickness
FFR	fractional flow reserve
IEL	internal elastic lamina
LCR	lipid-to-cap ratio
LPB	lipidic plaque burden
MACE	major adverse cardiovascular events
MLA	minimum lumen area
OCT	optical coherence tomography
QCA	quantitative coronary angiography
RWS	radial wall strain
SWS	superficial wall strain and stress
TCFA	thin-cap fibroatheroma

Introduction

Notwithstanding the relentless development of alternative diagnostic tools and techniques, coronary angiography (CAG) remains the cornerstone for the diagnosis of coronary artery disease (CAD). All other diagnostic modalities aim to identify patients who should be referred for CAG or undergo additional intracoronary imaging and physiological evaluation to further refine the CAG findings. CAG detects the presence of atherosclerotic plaque based on the imprint left on the vessel contour, but it offers limited information about prognostically important plaque composition and features of vulnerability^{1,2}.

Coronary strain, defined as the deformation caused on the vessel wall by the circumferential tensile stress derived from the pulsatile arterial pressure, is directly dependent on the tissue stiffness and hence on the plaque composition³⁻⁶. Plaque components associated with vulnerability, like the presence of lipids or macrophages, result in high strain values, whilst plaque components stabilising the plaque, like fibrous tissue or calcium, result in low strain values^{3,5-7}. Therefore, the presence of high-strain spots in the coronary arteries might estimate the plaque propensity to cause an acute coronary syndrome⁸. Under these premises, a reduction of high-strain spots after medical treatment has been considered as a surrogate for reduction of the lipidic plaque burden (LPB) and stabilisation of the plaque⁹⁻¹¹. Coronary strain can be calculated by means of elastography and palpography, both methods based on intravascular ultrasound (IVUS)^{3-6,8}. Coronary angiography can, however, estimate superficial wall strain and stress (SWS)^{12,13}, which consists of 4 different vectors, one of them being radial wall strain (RWS)¹⁴, but this approach requires a substantially complex and time-consuming methodology, including the analysis of 2 angiographic views without vessel overlap, which is not always possible.

Based on our findings from a previous finite element analysis study¹⁵, a novel method was proposed to directly calculate RWS from a single angiographic projection. Aided by artificial intelligence (AI), RWS can provide a simplified and cost-effective

tool to assess the biomechanical characteristics of the underlying plaque. We have recently shown that an optical coherence tomography (OCT)-derived lipid-to-cap ratio (LCR) >0.33, as an index of plaque vulnerability, could identify patients at high risk of adverse cardiovascular events caused by non-culprit plaque at the index procedure¹⁶. Encouraged by these promising findings, we are now evaluating the association of RWS with plaque composition, the LCR and other vulnerability indices by OCT.

Methods

STUDY DESIGN AND PATIENT POPULATION

Post hoc analysis of imaging data from a previously published single-centre study¹⁷ included all patients undergoing coronary angiography, fractional flow reserve (FFR) and OCT examination of non-culprit stenoses at Wakayama Medical University Hospital (Wakayama, Japan). Intracoronary nitroglycerine was systematically given to patients prior to angiography. Patients were excluded if balloon predilatation was performed prior to OCT imaging. For inclusion, the index lesions had to meet the following angiographic criteria: 1) lie in one of the 3 main coronary arteries; 2) intermediate stenosis; 3) a reference lumen diameter ≥ 2 mm. Index lesions were excluded from the analysis if: 1) tandem lesions, diffuse stenoses or in-stent restenosis in the interrogated vessels were present; 2) there was insufficient angiographic image quality, including full contrast filling less than 1 cardiac cycle, excessive overlap, foreshortening, or severe distortion; 3) OCT did not cover the entire lesion; 4) myocardial bridge was detected in the interrogated vessel; 5) vessel spasm or injury during OCT imaging was present; 6) there was insufficient OCT image quality including poor lumen visibility or severe artefacts; or 7) substantial thrombosis was identified by OCT.

Anonymised angiographic and OCT images were analysed at an independent core laboratory (CardHemo, Med-X Research Institute, Shanghai Jiao Tong University, Shanghai, China) by experienced analysts. The investigators analysing the angiography were blinded to the OCT results and vice versa.

The institutional review board of Wakayama Medical University approved the *post hoc* analysis of the data for this study and informed consent was waived. The study was conducted in accordance with the Declaration of Helsinki and the principles of Good Clinical Practice for human research.

CAG AND OCT IMAGE ACQUISITION

Angiographic images were obtained at 15 frames/sec on mono-plane or biplane X-ray angiogram (Allura Xper FD¹⁰; Philips).

OCT images were acquired with frequency-domain OCT systems (ILUMIEN or OPTIS; Abbott) at a frame rate of 100 or 180 frames/sec, respectively, using a non-occlusive technique.

RWS AND ANGIOGRAPHIC ANALYSIS

Analysis of angiography-based RWS and quantitative coronary angiography (QCA) was performed with AngioPlus Core software version 3.0 (Pulse Medical), following standard operating

procedures (**Supplementary Appendix 1**). The analyst selected the angiographic projection at end-diastole with minimal overlap and foreshortening for lesion analysis. Then, the software automatically selected 3 other frames with the least motion artefact at different periods of the cardiac cycle coregistered with electrocardiogram (ECG): early-systole, end-systole and mid-diastole. The lumen contours of the interrogated vessels were automatically delineated on these selected frames by means of AI and coregistered with the lumen contours at the other corresponding frames, thus generating a map of lumen diameters along the interrogated segments throughout the cardiac cycle; i.e., the lumen diameters of different cardiac phases were matched at every longitudinal position of the interrogated vessel (**Central illustration A**). RWS was calculated as the relative diameter deformation over the cardiac cycle for each position:

$$\text{RWS} = (\text{largest diameter} - \text{smallest diameter}) / \text{largest diameter}$$

Lesion RWS (dimensionless) was defined as the maximum RWS (RWS_{max}) along the interrogated lesion.

COLOCALISATION BETWEEN ANGIOGRAPHIC RWS_{max} AND OCT-DERIVED MAXIMUM LCR

CAG and OCT images were coregistered using the methodology that has been previously reported and validated¹⁸. Briefly, the lumen dimensions at different positions and their relative distances from each automatically detected side branch were extracted as input for a non-rigid point matching algorithm, which was able to correct for the non-linear longitudinal movement of the OCT image catheter caused by cardiac motion. This method showed a coregistration accuracy of 96%, with a median geographic matching error of 0.32 mm (interquartile range [IQR]: 0.00-0.56 mm) in our previous study using the same dataset¹⁸ (**Central illustration B**). After the coregistration, each longitudinal position of the OCT cross section was matched to an angiographic centreline point. Each plaque was divided into 3 segments along the longitudinal axis according to OCT images: throat segment, including the MLA position and the stenotic segments extending 1.5 mm proximal and 1.5 mm distal to the MLA; and proximal and distal stenotic segments (**Central illustration B**), defined as the upstream and downstream regions of the throat segment, up to the boundary between the plaque and the normal segment. Finally, the RWS and LCR within the same coregistered segment were separately and independently evaluated on CAG and OCT images (**Central illustration B**).

OCT ANALYSIS

Lumen morphology and plaque characterisation were automatically analysed from OCT images using AI-assisted software, OctPlus version 2.0 (Pulse Medical), as previously described¹⁹. Briefly, the lumen contours of the coregistered OCT cross sections were automatically delineated and the contour of the internal elastic lamina (IEL) was then identified or extrapolated from adjacent cross sections and prior knowledge of the shape of the media layer. The plaque composition for each OCT cross section was then automatically analysed and delineated in the region encompassed between the IEL and the lumen contour, using AI. Plaque

burden was defined as the surface of the IEL minus the lumen surface per cross section. The proportions of lipids, fibrous tissue and calcium within the plaque were then calculated per cross section and expressed as volumes from the 3D reconstruction¹⁹.

The following parameters of plaque vulnerability were automatically derived from the quantitative plaque characterisation in each cross section: fibrous cap thickness (FCT); lipid angle, defined as the angle encompassed by the lipid arc, measured from the gravitational centre of the lumen; LPB, defined as the proportion of lipidic plaque surface related to the IEL surface; and LCR, defined as LPB divided by FCT¹⁶ (**Central illustration C**). The plaque LCR was defined as the maximum LCR along the interrogated plaque. Plaques with an FCT <65 μm and lipid angle >180° were defined as thin-cap fibroatheroma (TCFA), according to previously reported criteria². In addition, other validated and prognostically relevant OCT features of plaque vulnerability were measured, including FCT <65 μm , minimum lumen area (MLA) <3.5 mm², lipid arc >180° and plaque burden >70%^{1,2}.

With the same software, the so-called optical flow ratio (OFR) was obtained to quantify the physiological significance of coronary stenosis. We have previously shown that the OFR correlates closely with wire-based FFR^{17,20,21}.

STATISTICAL ANALYSIS

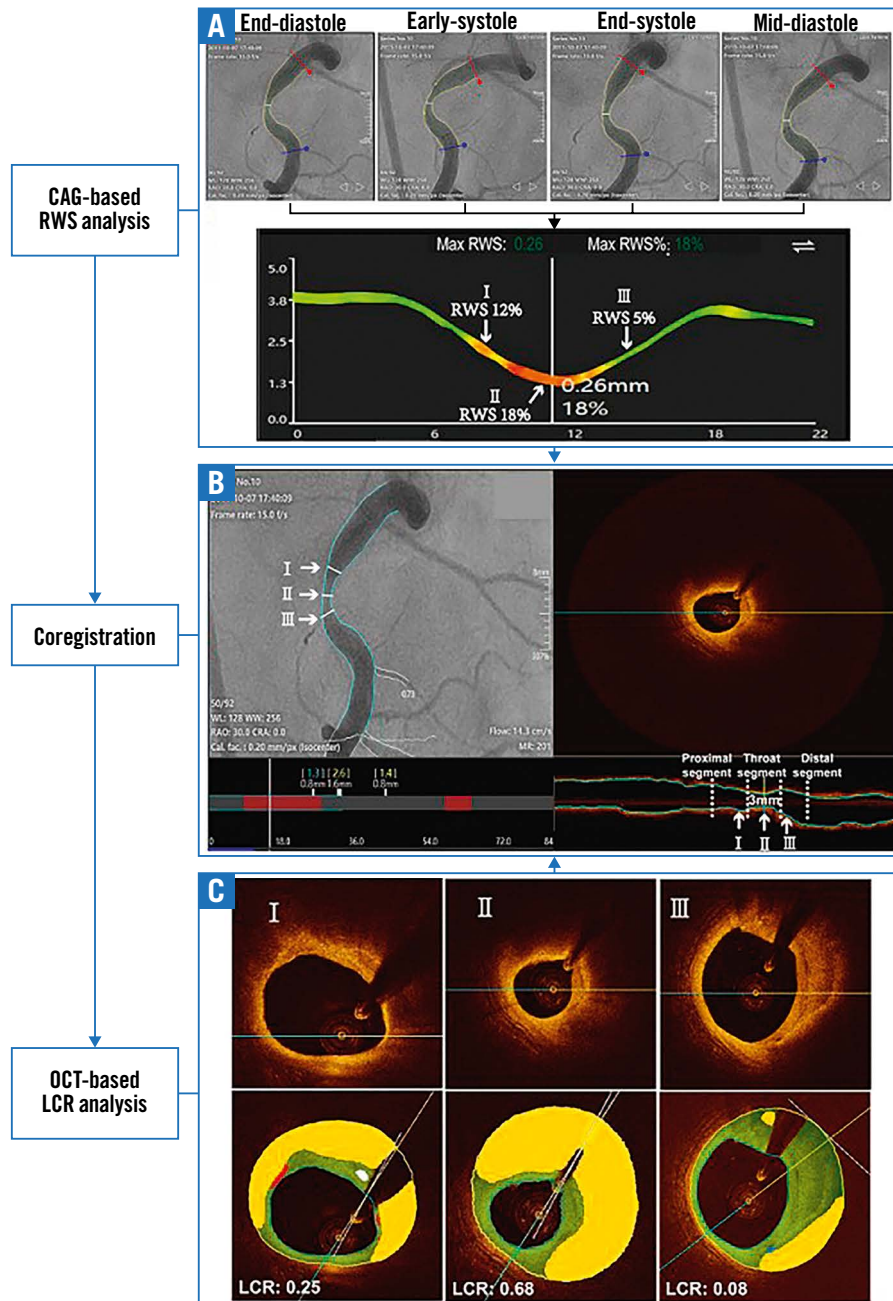
Descriptive statistics for continuous variables were expressed as mean \pm SD, if normally distributed, or as median (IQR), if not. Categorical variables were reported as number (percentage). Clinical characteristics were analysed on a per-patient basis, while plaque descriptors were reported on a per-vessel basis. Normal distribution was tested with the Shapiro-Wilk test. Correlation was evaluated using the Pearson correlation, if the variables were normally distributed, otherwise by means of the Spearman correlation. The chi-square test was used for distribution difference between the RWS_{max} and maximum LCR. Diagnostic performance was evaluated using the area under the curve (AUC) by receiver operating characteristic (ROC) analysis. The Youden index was used as the criterion to determine the best cut-off value of the RWS_{max} for the prediction of the LCR >0.33¹⁶ and TCFA. A sensitivity analysis, which divided the present study population into a derivation cohort and a validation cohort, was performed to test the consistency of the cut-off value of the RWS_{max} for predicting an LCR >0.33 when comparing with the result from the entire population. Inter- and intra-observer variability was assessed by means of the intraclass correlation coefficient for the absolute value (ICCa). All statistical calculations were performed with MedCalc Statistical Software version 19.2.6 (MedCalc Software bv). A 2-sided p-value <0.05 was considered statistically significant.

Results

BASELINE CLINICAL AND LESION CHARACTERISTICS

Altogether, 277 patients were enrolled in the original study¹⁷, but 41 patients were excluded due to balloon predilatation prior to OCT acquisition. Therefore, images from 236 patients (298 vessels)

CENTRAL ILLUSTRATION Coregistration and analysis of RWS and LCR.



A) The method for computation of RWS. White arrows show 3 representative positions at the proximal, throat, and distal segments with the computed RWS values (I, II, and III). B) Coregistration between CAG and OCT. White arrows on the left angiographic image and the right OCT longitudinal image show the same 3 representative positions as A (I, II, and III). The white dashed lines indicate the definition of the 3 segments. C) Corresponding OCT and tissue characterisation results at the same representative positions (I, II, and III). Position I at the proximal segment has an RWS of 12% and LCR of 0.25. Position II at the throat segment has an RWS of 18% and LCR of 0.68. Position III at the distal segment has an RWS of 5% and LCR of 0.08. CAG: coronary angiography; LCR: lipid-to-cap ratio; OCT: optical coherence tomography; RWS: radial wall strain

were screened at the core laboratory. After application of the pre-defined inclusion and exclusion criteria, 114 patients (124 vessels) were analysed (Figure 1).

Baseline demographic and plaque characteristics are shown in Table 1 and Table 2. In the study population, 49 (43.0%) patients had prior myocardial infarction (MI), and 66 (57.9%) patients had

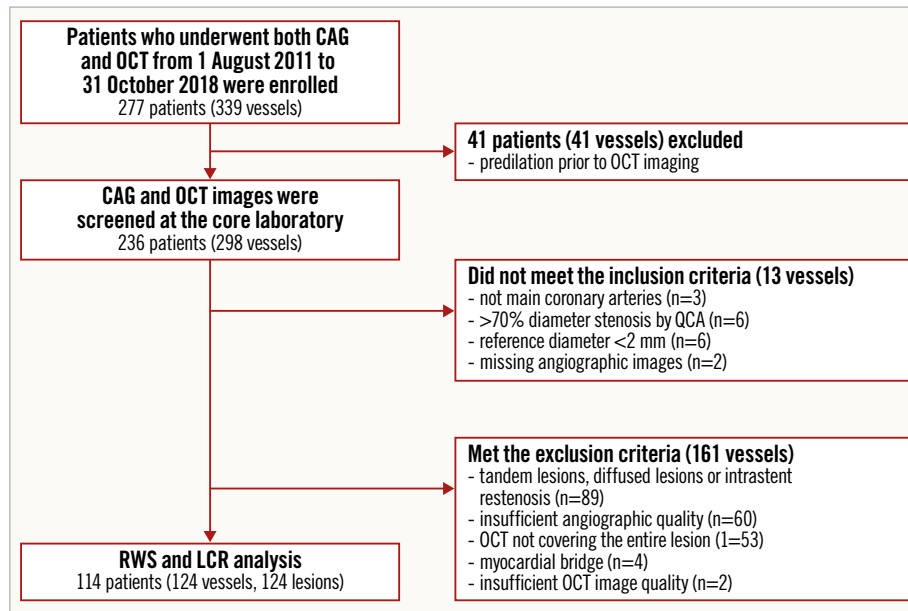


Figure 1. Study flow chart. CAG: coronary angiography; LCR: lipid-to-cap ratio; OCT: optical coherence tomography; QCA: quantitative coronary angiography; RWS: radial wall strain

prior percutaneous coronary intervention (PCI) in another vessel. The RWS_{max} in the index plaques showed a median value of 12% (IQR: 10-15%). Absolute lumen diameter change over the cardiac cycle was 0.25 (0.21-0.33) mm. Fourteen out of 124 plaques (11.3%) met TCFA criteria, and 57 plaques (46.0%) had $LCR > 0.33$. The average time for analysis of the RWS_{max} after selecting the angiographic image run was 57 (39-82) seconds.

Table 1. Baseline demographic characteristics.

	Patients (N=114)
Patient characteristics	
Age*, years	69±10
Men, n (%)	86 (75.4)
Diabetes mellitus, n (%)	39 (34.2)
Hypertension, n (%)	89 (78.1)
Hyperlipidaemia, n (%)	82 (71.9)
Smoking, n (%)	28 (24.6)
Family history of CAD, n (%)	25 (21.9)
Previous MI, n (%)	49 (43.0)
Previous PCI, n (%)	66 (57.9)
Previous CABG, n (%)	0 (0)
Clinical presentation	
Silent ischaemia, n (%)	55 (48.2)
Stable angina, n (%)	37 (32.5)
Unstable angina, n (%)	12 (10.5)
NSTEMI, n (%)	1 (0.9)
Others, n (%)	9 (7.9)
*Expressed as mean and standard deviation. CABG: coronary artery bypass grafting; CAD: coronary artery disease; MI: myocardial infarction; NSTEMI: non-ST-segment elevation myocardial infarction; PCI: percutaneous coronary intervention	

Table 2. Baseline plaque characteristics.

	Lesions (N=124)
Vessel distribution	
LAD, n (%)	72 (58.1)
RCA, n (%)	18 (14.5)
LCx, n (%)	34 (27.4)
QCA parameters	
Lesion length [†] , mm	10.9 (7.5-13.5)
Diameter stenosis*, %	35±12
Reference diameter [†] , mm	2.5 (1.8-3.5)
Minimal diameter [†] , mm	1.7 (1.5-2.1)
RWS related	
Absolute lumen diameter change [†] , mm	0.25 (0.21-0.33)
RWS_{max} [†] , %	12 (10-15)
Proximal segment [†]	11 (10-15)
Throat segment [†]	14 (10-15)
Distal segment [†]	11 (10-15)
OCT-related parameters	
Maximum lipid angle [†] , °	149 (116-197)
Minimum fibrous cap thickness [†] , μm	90 (71-112)
Minimum lumen area [†] , mm ²	2.05 (1.47-2.71)
Plaque burden*, %	58.0±6.4
Lipidic plaque burden [†] , %	19.9 (14.3-24.8)
Fibrous plaque burden [†] , %	29.3 (24.2-35.1)
Calcium burden [†] , %	2.0 (0.7-5.3)
Maximum LCR [†]	0.31 (0.17-0.43)
TCFA, n (%)	14 (11.3)
*Expressed as mean and standard deviation. [†] Expressed as median and interquartile range. LAD: left anterior descending; LCR: lipid-to-cap ratio; LCx: left circumflex artery; OCT: optical coherence tomography; RCA: right coronary artery; RWS: radial wall strain; TCFA: thin-cap fibroatheroma	

CORRELATION BETWEEN RWS_{max} , PLAQUE COMPOSITION AND PARAMETERS OF VULNERABILITY

Figure 2 shows a representative example with RWS_{max} and plaque parameters. RWS_{max} moderately correlated with the LCR ($r=0.584$; $p<0.001$), LPB ($r=0.411$; $p<0.001$) and maximum lipid arc ($r=0.276$; $p=0.002$). A negative correlation was found between the RWS_{max} and FCT ($r=-0.439$; $p<0.001$) and fibrous plaque burden ($r=-0.306$; $p<0.001$). Conversely, no significant correlation was found between the RWS_{max} and calcium burden ($r=-0.031$; $p=0.731$) (**Supplementary Figure 1**). For lesions with different physiological characteristics (classified according to the OFR), the RWS_{max} and OCT variables showed similar correlations as in the total sample (**Supplementary Table 1**).

Lesions with an LCR >0.33 have a higher RWS_{max} (14% [13-16] versus 10% [9-12]; $p<0.001$) and larger absolute lumen diameter change (0.31 mm [0.25-0.37] versus 0.22 mm [0.19-0.26]; $p<0.001$), compared to lesions with an LCR ≤ 0.33 (**Supplementary Table 2**). These lesions also have a thinner fibrous cap thickness (71 μm [57-90] versus 104 μm [90-146]; $p<0.001$) and larger maximum lipid angle (187° [150-227] versus 122° [92-158]; $p<0.001$).

Conversely, lesions with an LCR ≤ 0.33 had more fibrous plaque (32.0% [25.4-36.6] versus 26.0% [23.0-31.0]; $p<0.001$) (**Supplementary Table 2**). Notably, in the physiologically non-significant lesions (defined by an OFR ≥ 0.80), an $RWS_{max} >12\%$, LCR >0.33 , and TCFA represented 37.5%, 40.6%, and 12.5% of this cohort, respectively (**Supplementary Table 3**).

PLAQUE MORPHOLOGY, VULNERABILITY AND COMPUTATIONAL PHYSIOLOGY

When stratified by RWS_{max} , the MLA, lesion length and percent diameter stenosis (%DS) were comparable in the lesions with and without $RWS_{max} >12\%$. However, lesions with $RWS_{max} >12\%$ had a higher prevalence of TCFA (22.0% versus 1.5%; $p<0.001$), thinner fibrous cap thickness (71 μm vs 101 μm ; $p<0.001$), larger lipidic plaque burden (23.3% vs 15.4%; $p<0.001$), a higher maximum LCR (0.41 vs 0.18; $p<0.001$) and lower OFR (0.77 vs 0.83; $p=0.004$) compared to lesions with $RWS_{max} \leq 12\%$ (**Table 3**). Lesions with an $RWS_{max} \leq 12\%$ had more fibrous plaque.

COLOCALISATION BETWEEN RWS_{max} AND MAXIMUM LCR

In 98 (79%) lesions, there was perfect colocalisation of segments with the RWS_{max} and maximum OCT-derived LCR (**Supplementary Table 4**). Specifically, the maximum LCR localised in the proximal segment in 36%, the throat in 43% and in the distal segment in 21%, as compared to an RWS_{max} in 31, 46 and 23% of the same segments ($p=0.638$), respectively.

DIAGNOSTIC PERFORMANCE OF RWS_{max} FOR DETECTING FEATURES OF PLAQUE VULNERABILITY

The optimal strain cut-off value for the prediction of an LCR >0.33 (AUC=0.86, 95% confidence interval [CI]: 0.78-0.91) and TCFA (AUC=0.72, 95% CI: 0.63-0.80) was an $RWS_{max} >12\%$. The AUC in identifying plaques with simultaneous presence of FCT $<65 \mu\text{m}$,

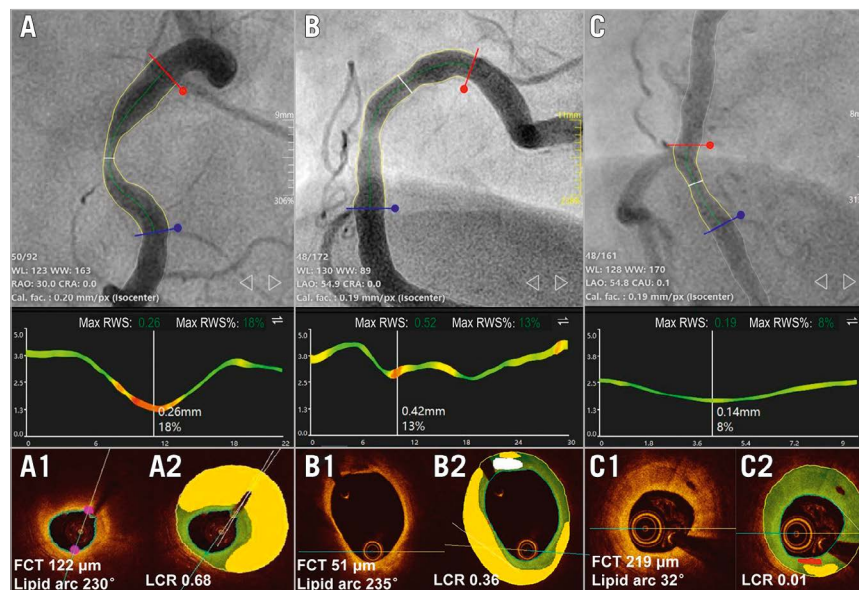


Figure 2. Representative examples of RWS_{max} and OCT-defined plaque characteristics. Coronary angiography showed 3 moderate lesions in the 3 RCA vessels (A, B, and C) with the corresponding RWS_{max} analyses and OCT plaque characterisation shown below, where the areas of lipid plaque, fibrotic tissue, calcified plaque and macrophages were presented in yellow, green, white and red, respectively. The white lines in the middle panels show the position with the RWS_{max} . The RWS_{max} derived from angiographic images was the highest for A (18%), followed by B (13%) and C (8%). OCT showed that there was a large lipid plaque but not defined as TCFA for A, while the LCR was 0.68 (A1-A2). B had TCFA but the LCR was lower than A, due to a smaller lipidic burden (B1-B2). C had the lowest LCR due to dominating fibrous plaque composition (C1-C2). FCT: fibrous cap thickness; LCR: lipid-to-cap ratio; RCA: right coronary artery; RWS: radial wall strain; TCFA: thin-cap fibroatheroma

Table 3. Comparison of plaque parameters of index lesions with different RWS_{max}*

	RWS _{max} >12% (n=59)	RWS _{max} ≤12% (n=65)	p-value
Absolute lumen diameter change*, mm	0.32 (0.25-0.37)	0.21 (0.19-0.26)	<0.001
Plaque burden*, %	60.0 (55.4-65.0)	56.3 (52.0-60.8)	0.002
Lipidic plaque burden*, %	23.3 (19.4-27.4)	15.4 (11.0-20.3)	<0.001
Fibrous plaque burden*, %	28.0 (23.6-31.5)	31.4 (24.9-36.2)	0.020
Calcified plaque burden*, %	2.0 (0.7-4.4)	2.1 (0.5-6.0)	0.779
Minimum lumen area*, mm ²	2.0 (1.3-2.5)	2.1 (1.7-3.1)	0.050
Minimum fibrous cap thickness*, μm	71 (58-92)	101 (89-150)	<0.001
Maximum lipid arc*, °	179 (134-210)	128 (92-167)	<0.001
TCFA, n (%)	13 (22.0)	1 (1.5)	<0.001
LCR*	0.41 (0.35-0.53)	0.18 (0.13-0.26)	<0.001
LCR >0.33, n (%)	49 (83.2)	8 (12.3)	<0.001
OFr*	0.77 (0.71-0.83)	0.83 (0.76-0.87)	0.004
Lesion length*, mm	11.4 (8.6-13.6)	10.4 (7.4-13.1)	0.329
Diameter stenosis*, %	36 (30-46)	33 (26-43)	0.120
Reference diameter*, mm	2.9 (2.4-3.1)	2.9 (2.4-3.2)	0.818
Minimum lumen diameter*, mm	1.7 (1.4-2.0)	1.8 (1.6-2.1)	0.020

*Expressed as median and interquartile range. LCR: lipid-to-cap ratio; OFr: optical flow ratio; RWS: radial wall strain; TCFA: thin-cap fibroatheroma

maximum lipid arc >180° and MLA <3.5 mm² was 0.82 (95% CI: 0.74-0.88; p<0.001) (**Figure 3**). The diagnostic performance of the RWS_{max} with these cut-off values is shown in **Supplementary Table 5**. When including only non-flow limiting coronary lesions with an OFr ≥0.80 in the analysis, an RWS_{max} >12% also had a good accuracy in predicting an LCR >0.33 (AUC=0.80, 95% CI: 0.68-0.89) (**Supplementary Figure 2**). In sensitivity analysis, the best cut-off value of the RWS_{max} for predicting an LCR >0.33 was also found at 12%, exactly the same as the best cut-off value

when using the entire study population (**Supplementary Figure 3**). The performance of using this cut-off value in the validation cohort showed similar performance of the RWS_{max} in predicting an LCR >0.33 (**Supplementary Table 6**).

REPRODUCIBILITY OF RWS_{MAX}

The inter- and intra-observer ICCa values of the RWS_{max} were 0.856 (95% CI: 0.720-0.929) and 0.926 (95% CI: 0.895-0.948), respectively.

Discussion

The main findings of this study are: 1) RWS can be estimated by means of coronary angiography when analysing the dynamic changes in diameter over the cardiac cycle and aided by artificial intelligence for the delineation of the luminal contour. 2) Plaque strain derived from CAG correlated significantly with validated features of plaque vulnerability, whilst it correlated negatively with the fibrous plaque. 3) When dividing the lesion into proximal, throat, and distal segments, the RWS_{max} colocalised well with the maximum LCR in the same segment. 4) In the absence of physiologically significant stenosis, roughly 1/3 of the intermediate lesions had a high RWS_{max} or high LCR.

Coronary strain has been calculated by IVUS-based methods hitherto, namely elastography and palpography, the latter being the elastography of the most adluminal layers of the vessel wall^{3-6,8}. Elasto-palpography was initially developed before the advent of virtual histology, OCT or spectroscopy and aimed to detect lipid-rich plaques that were known to be harbingers of acute coronary syndromes²². The biomechanical concept was successful, as high strain correlated with plaque elements linked to vulnerability, like lipids or macrophages, whilst low strain correlated with components linked to plaque stabilisation, like fibrous tissue or calcium^{3,5-7}. The presence of high-strain spots was associated with an increased incidence of acute coronary syndromes⁸ and a reduction of high-strain spots has been considered as a surrogate for plaque

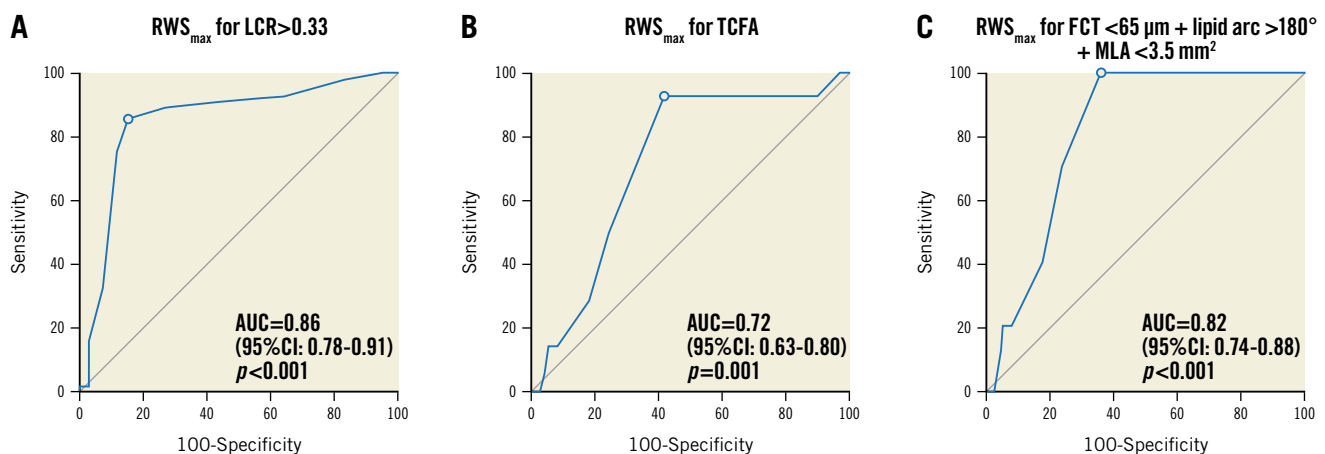


Figure 3. ROC curve analysis and predictive value of RWS_{max} for OCT-derived plaque parameters. AUC: area under the curve; CI: confidence interval; FCT: fibrous cap thickness; LCR: lipid-to-cap ratio; MLA: minimum lumen area; ROC: receiver operating characteristics; RWS: radial wall strain; TCFA: thin-cap fibroatheroma

stabilisation⁹⁻¹¹. Nonetheless, the advent of other invasive techniques for detailed plaque characterisation has relegated elastopalpography to a marginal role, with, currently, very limited use. In addition, cardiac motion artefacts remain a significant limitation to IVUS-based strain calculations, jeopardising its accuracy. Coronary strain derived from finite element analysis circumvents the above-mentioned limitations but is somehow limited by long and laborious analytical procedures. Our previously reported approach based on OCT shows a good correlation between lumen dimensional change with both plaque stress and lipid plaque area, providing the first-in-human indication that angiography-derived RWS allows the assessment of the biomechanical characteristics of the underlying plaque¹⁵. Of note, our method is supported by AI which allows an automation of many cumbersome and repetitive tasks, thus turning complex approaches that were once considered prohibitive into clinically usable methods^{18,23}. The current study is paradigmatic of the power of AI to transform medical diagnosis. The analysis of the dynamic changes in coronary luminal diameters over the cardiac cycle would require the analysis of too many angiographic frames to be performed manually, but the task becomes reliable when undertaken by an AI algorithm. The first proof-of-concept study should be validating the correspondence between angio-based RWS_{max} and features of plaque vulnerability. In the present study, AI was also applied for automated plaque characterisation in OCT cross sections. For OCT segments with high light attenuation precluding the unambiguous delineation of vascular structures, the media contour could be extrapolated from our deep learning algorithm by incorporating the information from adjacent OCT cross sectional images and the prior knowledge about the shape of media layer¹⁸. Recently, Gerbaud et al²⁴ also reported increased accuracy in the quantification of plaque burden on OCT by combining adaptive attenuation compensation and exponentiation for contrast enhancement. The results of this first pilot study are highly encouraging: a high RWS_{max} correlates well with features of vulnerability, whilst a low RWS_{max} correlates well with features of stability, like fibrous tissue or FCT. Our findings are biologically plausible and in line with previous IVUS investigations of coronary strain^{3-6,8}. In addition, exact concordance in colocalised RWS_{max} and maximum LCR within each lesion was observed in 79% of cases. These findings confirm that “softer” spots with thin fibrous cap and high lipid content are deformable. However, RWS is a biomechanical parameter concurrently determined by the interaction between plaque composition and the local biomechanical environment, including heart contraction and blood pressure changes, thus resulting in modest correlations with imaging features such as lipid plaque burden and thin fibrous cap. Similar results were obtained in studies exploring correlations between other biomechanical factors (e.g., plaque structural stress) and OCT- or IVUS-derived vulnerable features^{6,8,15,25}. In addition, the angiographic images were exported with a reduced image size (512×512 pixels) for analysis, resulting in an image resolution of 0.2 mm/pixel. Of all the lesions, 11 (9%) had a high RWS_{max} of >12% and an absolute lumen diameter change greater

than 0.4 mm, that is, a difference of more than 2 pixels. Of note, all modern X-ray angiograms have an image size $\geq 1,024 \times 1,024$ pixels. If the original image size could be used for RWS analysis, the spot with high RWS would have ≥ 4 pixels change in lumen diameter during the cardiac cycle.

The opportunity to estimate plaque wall strain from a simple diagnostic coronary angiogram reveals hidden information which can be extracted from this ubiquitous examination for the diagnosis and management of CAD. QCA, computational physiology²⁶⁻²⁸ and SWS¹²⁻¹⁴ have provided additional angiographic content, with a potential impact on clinical outcomes. The recent COMBINE OCT-FFR study demonstrated that non-flow limiting coronary plaques with TCFA had unfavourable clinical outcomes compared to non-TCFA lesions²⁹. The present study also found that in the absence of physiologically significant lesions, roughly 1/3 of the intermediate lesions had an $RWS_{max} > 12\%$ or $LCR > 0.33$. Although preventative stenting of vulnerable plaques remains controversial, vulnerability assessments appear to confer incremental prognostic value in the presence of coronary lesions with preserved FFR²⁹. Accordingly, improved prognosis of vulnerable and non-flow limiting plaques could be achieved by individualised plaque passivation following intensive medication, irrespective of functional significance. Of note, both RWS and single-view quantitative flow ratio (QFR), namely μQFR ³⁰, have been incorporated into the same AngioPlus software. RWS computation can be performed immediately after the μQFR analysis (**Supplementary Appendix 1**). It remains to be demonstrated in a prospective study to which extent the combination of RWS and QFR can improve risk stratification for mild lesions with vulnerability features but preserved haemodynamics. Conversely, the high negative predictive value of RWS in identifying TCFA would further support the use of RWS in enhancing the safety of PCI deferral in the presence of a preserved QFR. These are currently appealing hypotheses worth exploring, but specific evidence must be generated in upcoming clinical studies.

Study limitations

This was a retrospective single-centre study, with all the limitations inherent to this design. Although strict inclusion and exclusion criteria were applied for analysis, selection bias cannot be ruled out, especially with respect to upstream clinical decisions to perform intracoronary imaging, or not. Likewise, the generalisability of the results to more severe lesions, especially in the presence of stress-induced or even resting translesional pressure gradients, needs to be addressed in future studies. In addition, due to the retrospective nature of the current study, 42% of the vessels were excluded, mainly because of previously implanted stents or unsatisfactory angiography quality. Future prospective studies testing the value of the RWS_{max} in all-comer patient populations are warranted.

This was a pilot study to explore the relation between plaque composition, vulnerability and RWS_{max} as previously reported by IVUS studies^{3-6,8}. No head-to-head comparison with strain

calculated by means of elasto-palpography (i.e., IVUS) was performed in the current study, but reliable measurement of elasto-palpography from IVUS requires the absence of longitudinal movement between the IVUS probe and the imaging cross section, which is technically challenging due to cardiac motion.

In the present study, we found no association between a low RWS_{max} and calcium. This could be explained by low (3.5%) calcium content in the studied plaque, disabling any opportunity to detect a potential association. The precise interaction between calcium presence and location and RWS_{max} may require further analysis. A large calcific plate occupying 1 quadrant within a large lipidic pool, will result in higher strain values than a small per-luminal calcific ring, constraining any dynamic change in lumen diameters to negligible values. The association between calcium and strain might be more dependent on the distribution than on the amount of mineral deposited. This hypothesis will deserve specific appraisal in future dedicated larger-size studies. Of note, the correlation between the RWS_{max} and the presence of macrophages was not evaluated in the current study, considering the suboptimal precision of the deep learning algorithm in identifying areas infiltrated with macrophages¹⁸.

Although RWS_{max} has distinct advantages, the method also has some intrinsic shortcomings. The performance of RWS_{max} will inevitably be impacted by changes in the analysed angle (during vessel motion and twist), the angiographic projection and quality of the angiographic images. Prospective studies to investigate which angiographic image acquisition settings are needed to optimise the results of RWS analysis are warranted. It is possible that the changes in luminal diameter will only be partially detected in eccentric plaque. Finally, RWS_{max} does not assess lumen deformation due to vessel elongation and torsion.

Conclusions

Angiography-derived RWS_{max} was significantly correlated with plaque composition and known OCT features of plaque vulnerability in patients with intermediate coronary stenosis. RWS_{max} appears to be a cost-efficient tool to evaluate the mechanical properties of non-culprit plaque during diagnostic angiography.

Impact on daily practice

This novel method to derive radial wall strain from a single projection of coronary angiography was correlated with plaque composition and markers of plaque vulnerability by OCT. Plaque strain made available during routine angiography may complement angiography-based physiological assessments in order to make clinically relevant decisions in the cath lab, while optimising costs and time requirements needed for the implementation of more complex techniques.

Funding

S. Tu would like to acknowledge the support of the Natural Science Foundation of China (Nos. 82020108015 and 81871460).

W. Wijns would like to acknowledge support from the Science Foundation Ireland Research Professorship Award (15/RP/2765). L. Chen would like to acknowledge support from the Fund for Top Hospital and Specialty Excellence of Fujian Province.

Conflict of interest statement

S. Tu reports research grants and consultancy from Pulse Medical, during the conduct of the study. The other authors have no conflicts of interest to declare relevant to the contents of this paper.

References

- Stone GW, Maehara A, Lansky AJ, de Bruyne B, Cristea E, Mintz GS, Mehran R, McPherson J, Farhat N, Marso SP, Parise H, Templin B, White R, Zhang Z, Serruys PW; PROSPECT Investigators. A prospective natural-history study of coronary atherosclerosis. *N Engl J Med*. 2011;364:226-35.
- Prati F, Romagnoli E, Gatto L, La Manna A, Burzotta F, Ozaki Y, Marco V, Boi A, Fineschi M, Fabbicocchi F, Taglieri N, Niccoli G, Trani C, Versaci F, Calligaris G, Ruscia G, Di Giorgio A, Vergallo R, Albertucci M, Biondi-Zoccai G, Tamburino C, Crea F, Alfonso F, Arbustini E. Relationship between coronary plaque morphology of the left anterior descending artery and 12 months clinical outcome: the CLIMA study. *Eur Heart J*. 2020;41:383-91.
- de Korte CL, Pasterkamp G, van der Steen AF, Woutman HA, Bom N. Characterization of plaque components with intravascular ultrasound elastography in human femoral and coronary arteries in vitro. *Circulation*. 2000;102:617-23.
- de Korte CL, Siervogel MJ, Mastik F, Strijder C, Schaar JA, Velema E, Pasterkamp G, Serruys PW, van der Steen AF. Identification of atherosclerotic plaque components with intravascular ultrasound elastography in vivo: a Yucatan pig study. *Circulation*. 2002;105:1627-30.
- de Korte CL, Carlier SG, Mastik F, Doyley MM, van der Steen AFW, Serruys PW, Bom N. Morphological and mechanical information of coronary arteries obtained with intravascular elastography; feasibility study in vivo. *Eur Heart J*. 2002;23:405-13.
- Schaar JA, De Korte CL, Mastik F, Strijder C, Pasterkamp G, Boersma E, Serruys PW, Van Der Steen AF. Characterizing vulnerable plaque features with intravascular elastography. *Circulation*. 2003;108:2636-41.
- Cheng GC, Loree HM, Kamm RD, Fishbein MC, Lee RT. Distribution of circumferential stress in ruptured and stable atherosclerotic lesions. A structural analysis with histopathological correlation. *Circulation*. 1993;87:1179-87.
- Schaar JA, Regar E, Mastik F, McFadden EP, Saia F, Disco C, de Korte CL, de Feyter PJ, van der Steen AFW, Serruys PW. Incidence of high-strain patterns in human coronary arteries: assessment with three-dimensional intravascular palpography and correlation with clinical presentation. *Circulation*. 2004;109:2716-9.
- Van Mieghem CA, McFadden EP, de Feyter PJ, Bruining N, Schaar JA, Mollet NR, Cademartiri F, Goedhart D, de Winter S, Granillo GR, Valgimigli M, Mastik F, van der Steen AF, van der Giessen WJ, Sianos G, Backx B, Morel MA, van Es GA, Zalewski A, Serruys PW. Noninvasive detection of subclinical coronary atherosclerosis coupled with assessment of changes in plaque characteristics using novel invasive imaging modalities: the Integrated Biomarker and Imaging Study (IBIS). *J Am Coll Cardiol*. 2006;47:1134-42.
- Serruys PW, Garcia-Garcia HM, Buszman P, Erne P, Verheyse S, Aschermann M, Duckers H, Bleie O, Dudek D, Bøtker HE, von Birgelen C, D'Amico D, Hutchinson T, Zambanini A, Mastik F, van Es GA, van der Steen AF, Vince DG, Ganz P, Hamm CW, Wijns W, Zalewski A; Integrated Biomarker and Imaging Study-2 Investigators. Effects of the direct lipoprotein-associated phospholipase A(2) inhibitor darapladib on human coronary atherosclerotic plaque. *Circulation*. 2008;118:1172-82.
- Li Z, Wang L, Hu X, Zhang P, Chen Y, Liu X, Xu M, Zhang Y, Zhang M. Effect of rosuvastatin on atherosclerotic plaque stability: An intravascular ultrasound elastography study. *Atherosclerosis*. 2016;248:27-35.
- Wu X, von Birgelen C, Muramatsu T, Li Y, Holm NR, Reiber JHC, Tu S. A novel four-dimensional angiographic approach to assess dynamic superficial wall stress of coronary arteries in vivo: initial experience in evaluating vessel sites with subsequent plaque rupture. *EuroIntervention*. 2017;13:e1099-103.
- Wu X, Ono M, Kawashima H, Poon EKW, Torii R, Shahzad A, Gao C, Wang R, Barlis P, von Birgelen C, Reiber JHC, Bourantas CV, Tu S, Wijns W, Serruys PW, Onuma Y. Angiography-Based 4-Dimensional Superficial Wall Strain and Stress: A New Diagnostic Tool in the Catheterization Laboratory. *Front Cardiovasc Med*. 2021;8:667310.
- Gutiérrez-Chico JL. Superficial wall stress: the long awaited comprehensive biomechanical parameter to objectify and quantify our intuition. *Int J Cardiovasc Imaging*. 2018;34:863-5.

15. Huang J, Yang F, Gutiérrez-Chico JL, Xu T, Wu J, Wang L, Lv R, Lai Y, Liu X, Onuma Y, Tang D, Serruys PW, Wijns W, Tu S. Optical Coherence Tomography-Derived Changes in Plaque Structural Stress Over the Cardiac Cycle: A New Method for Plaque Biomechanical Assessment. *Front Cardiovasc Med.* 2021;8:715995.
16. Hong H, Jia H, Zeng M, Gutiérrez-Chico JL, Wang Y, Zeng X, Qin Y, Zhao C, Chu M, Huang J, Liu L, Hu S, He L, Chen L, William W, Yu B, Tu S. Risk Stratification in Acute Coronary Syndrome by Comprehensive Morphofunctional Assessment With Optical Coherence Tomography. *JACC: Asia.* 2022;2:460-472.
17. Huang J, Emori H, Ding D, Kubo T, Yu W, Huang P, Zhang S, Gutiérrez-Chico JL, Akasaka T, Wijns W, Tu S. Diagnostic performance of intracoronary optical coherence tomography-based versus angiography-based fractional flow reserve for the evaluation of coronary lesions. *EuroIntervention.* 2021;16:568-76.
18. Qin H, Li C, Li Y, Huang J, Yang F, Kubo T, Akasaka T, Xiao C, Gutiérrez-Chico JL, Tu S. Automatic Coregistration Between Coronary Angiography and Intravascular Optical Coherence Tomography: Feasibility and Accuracy. *JACC: Asia.* 2021;1:274-8.
19. Chu M, Jia H, Gutiérrez-Chico JL, Maehara A, Ali ZA, Zeng X, He L, Zhao C, Matsumura M, Wu P, Zeng M, Kubo T, Xu B, Chen L, Yu B, Mintz GS, Wijns W, Holm NR, Tu S. Artificial intelligence and optical coherence tomography for the automatic characterisation of human atherosclerotic plaques. *EuroIntervention.* 2021;17:41-50.
20. Yu W, Huang J, Jia D, Chen S, Raffel OC, Ding D, Tian F, Kan J, Zhang S, Yan F, Chen Y, Bezerra HG, Wijns W, Tu S. Diagnostic accuracy of intracoronary optical coherence tomography-derived fractional flow reserve for assessment of coronary stenosis severity. *EuroIntervention.* 2019;15:189-97.
21. Ding D, Yu W, Tauzin H, De Maria GL, Wu P, Yang F, Kotronias RA, Terentes-Printzios D, Wolfrum M, Banning AP, Meneveau N, Wijns W, Tu S. Optical flow ratio for assessing stenting result and physiological significance of residual disease. *EuroIntervention.* 2021;17:e989-98.
22. MacIsaac AI, Thomas JD, Topol EJ. Toward the quiescent coronary plaque. *J Am Coll Cardiol.* 1993;22:1228-41.
23. Zhao Q, Li C, Chu M, Gutiérrez-Chico JL, Tu S. Angiography-based coronary flow reserve: The feasibility of automatic computation by artificial intelligence. *Cardiol J.* 2021 Aug 6. [Epub ahead of print].
24. Gerbaud E, Weisz G, Tanaka A, Luu R, Osman HASH, Baldwin G, Coste P, Cognet L, Waxman S, Zheng H, Moses JW, Mintz GS, Akasaka T, Maehara A, Tearney GJ. Plaque burden can be assessed using intravascular optical coherence tomography and a dedicated automated processing algorithm: a comparison study with intravascular ultrasound. *Eur Heart J Cardiovasc Imaging.* 2020;21:640-52.
25. Costopoulos C, Huang Y, Brown AJ, Calvert PA, Hoole SP, West NEJ, Gillard JH, Teng Z, Bennett MR. Plaque Rupture in Coronary Atherosclerosis Is Associated With Increased Plaque Structural Stress. *JACC Cardiovasc Imaging.* 2017;10:1472-83.
26. Xu B, Tu S, Song L, Jin Z, Yu B, Fu G, Zhou Y, Wang J, Chen Y, Pu J, Chen L, Qu X, Yang J, Liu X, Guo L, Shen C, Zhang Y, Zhang Q, Pan H, Fu X, Liu J, Zhao Y, Escaned J, Wang Y, Fearon WF, Dou K, Kirtane AJ, Wu Y, Serruys PW, Yang W, Wijns W, Guan C, Leon MB, Qiao S, Stone GW; FAVOR III China study group. Angiographic quantitative flow ratio-guided coronary intervention (FAVOR III China): a multicentre, randomised, sham-controlled trial. *Lancet.* 2021;398:2149-59.
27. Tu S, Westra J, Adjedj J, Ding D, Liang F, Xu B, Holm NR, Reiber JHC, Wijns W. Fractional flow reserve in clinical practice: from wire-based invasive measurement to image-based computation. *Eur Heart J.* 2020;41:3271-9.
28. Tu S, Westra J, Yang J, von Birgelen C, Ferrara A, Pellicano M, Nef H, Tebaldi M, Murasato Y, Lansky A, Barbato E, van der Heijden LC, Reiber JH, Holm NR, Wijns W; FAVOR Pilot Trial Study Group. Diagnostic Accuracy of Fast Computational Approaches to Derive Fractional Flow Reserve From Diagnostic Coronary Angiography: The International Multicenter FAVOR Pilot Study. *JACC Cardiovasc Interv.* 2016;9:2024-35.
29. Kedhi E, Berta B, Roleder T, Hermanides RS, Fabris E, IJsselmuiden AJJ, Kauer F, Alfonso F, von Birgelen C, Escaned J, Camaro C, Kennedy MW, Pereira B, Magro M, Nef H, Reith S, Al Nooryani A, Rivero F, Malinowski K, De Luca G, Garcia Garcia H, Granada JF, Wojakowski W. Thin-cap fibroatheroma predicts clinical events in diabetic patients with normal fractional flow reserve: the COMBINE OCT-FFR trial. *Eur Heart J.* 2021;42:4671-9.
30. Tu S, Ding D, Chang Y, Li C, Wijns W, Xu B. Diagnostic accuracy of quantitative flow ratio for assessment of coronary stenosis significance from a single angiographic view: A novel method based on bifurcation fractal law. *Catheter Cardiovasc Interv.* 2021;97 Suppl 2:1040-7.

Supplementary data

Supplementary Appendix 1. Methods: SOP for μ QFR and RWS analysis, version 1.0.

Supplementary Table 1. Correlation coefficient between RWS_{max} and OCT variables.

Supplementary Table 2. Comparison of plaque parameters in groups with different plaque vulnerabilities defined by LCR.

Supplementary Table 3. Comparison of plaque parameters of index lesions in different vascular physiological environments defined by OFR.

Supplementary Table 4. Colocalisation rate of RWS_{max} with maximum LCR.

Supplementary Table 5. Diagnostic performance of $RWS_{max} > 12\%$ for LCR and TCFA.

Supplementary Table 6. Diagnostic performance of $RWS_{max} > 12\%$ for LCR > 0.33 in the derivation cohort.

Supplementary Figure 1. Correlation between RWS_{max} and OCT-derived plaque parameters.

Supplementary Figure 2. ROC analysis and predictive value of RWS_{max} for LCR > 0.33 in non-flow limiting lesions.

Supplementary Figure 3. ROC analysis in the derivation cohort.

The supplementary data are published online at:

<https://eurointervention.pconline.com/>

<doi/10.4244/EIJ-D-22-00537>



Supplementary data

Supplementary Appendix 1. Methods: SOP for μ QFR and RWS analysis, version

1.0.

The standard operation procedure (SOP) for the analysis of μ QFR and RWS based on a single angiographic image run using the AngioPlus Core software (version V3, Pulse Medical, Shanghai, China) has the following steps:

1. Import an angiographic image run with no overlap and minimal foreshortening to the interrogated lesions into the software;
2. The software automatically selects the vessel type. The analyst needs to confirm whether the vessel type is correct or not. If not, manually change the vessel type;
3. The software will then automatically quantify the flow velocity based on the contrast dye filling of the interrogated vessel and select the best image frame as Key Frame for analysis. Typically, the frame at the end-diastole without much panning is selected. The analyst should modify the Key Frame if the automatically selected frame does not optimally expose the lesions. The lesion should look the most severe and clear in the Key Frame compared with other image frames;
4. The software automatically delineates the lumen contour of the interrogated vessel and its side branches. The analyst should modify the lumen contours if lumen contours do not follow the true lumen edge, or the side branches if the side branches are not correctly delineated;
5. The software automatically reconstructs the step-down reference vessel size as if there was no stenosis, using the lumen size of the interrogated vessel and its side branches. The analyst should modify the positions of the proximal normal (PN) lumen and distal normal (DN) lumen if the automatically detected PN and DN are not in the positions with healthy lumen;
6. The μ QFR is computed and report at every location along the interrogated vessel and its side branches. The lesion with the most severe stenosis is detected and lesion-specific parameters including percent diameter stenosis, minimal lumen

diameter, and lesion length are reported;

7. The software automatically selects three additional image frames at different cardiac phases with sharp lumen contours and computes RWS at every location of the stenotic segment after co-registering the lumen contours of these four image frames. The analyst should change image frames for analysis if the image quality of the stenotic segment is suboptimal. If the lumen contours do not follow the true lumen edge in any of these image frames, the analyst should correct the contours. After correction, the software will re-compute RWS. The maximum RWS value will be reported.

Supplementary Table 1. Correlation coefficient between RWS_{max} and OCT variables.

	All lesions	Lesions with OFR<0.8	Lesions with OFR \geq 0.8
RWS _{max} and LCR*	0.584 (0.455 - 0.690, p<0.001)	0.511 (0.303 - 0.672, p<0.001)	0.654 (0.480 - 0.779, p<0.001)
RWS _{max} and minimum FCT*	-0.439 (-0.571 - 0.285, p<0.001)	-0.439 (-0.618 - -0.217, p<0.001)	-0.463 (-0.642 - -0.237, p<0.001)
RWS _{max} and maximum lipid arc*	0.276 (0.105 - 0.431, p=0.002)	0.242 (-0.004 - 0.461, p=0.054)	0.344 (0.099 - 0.550, p=0.007)
RWS _{max} and lipidic plaque burden*	0.411 (0.253 - 0.548, p<0.001)	0.264 (0.019 - 0.479, p=0.035)	0.518 (0.304 - 0.682, p<0.001)
RWS _{max} and fibrous plaque burden*	-0.306 (-0.457 - 0.137, p<0.001)	-0.118 (-0.354 - 0.131, p=0.351)	-0.260 (-0.482 - 0.006, p=0.045)
RWS _{max} and calcified plaque burden*	-0.031 (-0.206 - 0.146, p=0.731)	-0.185 (-0.412 - 0.064, p=0.143)	0.104 (-0.154 - 0.349, p=0.430)

* Expressed as median and interquartile range.

RWS: radial wall strain; OFR: optical flow ratio; LCR: lipid-to-cap ratio.

Supplementary Table 2. Comparison of plaque parameters in groups with different plaque vulnerabilities defined by LCR.

	LCR >0.33 (n=57)	LCR ≤0.33 (n=67)	p-value
RWS _{max} [*] , %	14 (13-16)	10 (9-12)	<0.001
RWS _{max} >12%, n (%)	48 (84.2%)	10 (14.9%)	<0.001
Absolute lumen diameter change*, mm	0.31(0.25-0.37)	0.22(0.19-0.26)	<0.001
OFR [*]	0.78 (0.73-0.85)	0.82 (0.75-0.86)	0.061
Plaque burden*, %	59.5 (55.2-63.6)	56.5 (52.1-61.3)	0.030
Lipidic plaque burden*, %	23.6 (20.2-28.8)	15.4 (10.9-20.1)	<0.001
Fibrous plaque burden*, %	26.0 (23.0-31.0)	32 (25.4-36.6)	<0.001
Calcified plaque burden*, %	1.8 (0.7-4.2)	2.2 (0.6-6.2)	0.506
Minimum lumen area*, mm ²	2.1 (1.3-2.6)	2.0 (1.6-2.9)	0.290
Minimal fibrous cap thickness*, μm	71 (57-90)	104 (90-146)	<0.001
Maximum lipid arc*, °	187 (150-227)	122 (92-158)	<0.001
TCFA, n (%)	13 (22.8)	1 (1.5%)	<0.001
Lesion length*,mm	11.3 (8.7-13.7)	10.6 (7.2-13.3)	0.356
Diameter stenosis*, %	35 (28-43)	33 (26-44)	0.371
Reference diameter*, mm	2.9 (2.5-3.2)	2.8 (2.4-3.2)	0.247

* Expressed as median and interquartile range.

RWS: radial wall strain; OFR: optical flow ratio; LCR: lipid-to-cap ratio; TCFA, thin-cap

fibroatheroma.

Supplementary Table 3. Comparison of plaque parameters of index lesions in different vascular physiological environments defined by OFR.

	OFR<0.8 (n=60)	OFR≥0.8 (n=64)	p-value
RWS _{max} [*] , %	14 (11-16)	11 (9-14)	0.008
RWS _{max} >12%, n (%)	35 (58.8)	24 (37.5)	0.021
Absolute lumen diameter change*, mm	0.26 (0.21-0.31)	0.25 (0.20-0.34)	0.785
Lesion length ^a , mm	10.2 (7.5-13.2)	11.0 (7.7-13.7)	0.557
Diameter stenosis*, %	34.5 (26.5-47.0)	35.0 (27.0-42.5)	0.545
Minimum lumen diameter*, mm	1.6 (1.4-2.01)	1.8 (1.7-2.1)	0.010
LCR*	0.33 (0.17-0.43)	0.29 (0.17-0.39)	0.591
LCR>0.33, n (%)	31 (51.7)	26 (40.6)	0.220
Minimal fibrous cap thickness*, μm	92 (70-111)	90 (71-113)	0.724
Maximum lipid arc*, °	146 (112-182)	149 (120-210)	0.456
TCFA, n (%)	6 (10%)	8 (12.5%)	0.039
Plaque burden*, %	62.0 (55.7-65.8)	68.6 (52.2-59.6)	<0.001
Lipidic plaque burden*, %	21.1 (15.0-25.5)	18.1 (14.0-23.3)	0.217
Fibrous plaque burden*, %	29.5(25.5-36.1)	28.6 (23.8-34.0)	0.373
Calcified plaque burden*, %	3.1 (0.6-5.4)	1.7 (0.7-4.9)	0.601
Minimum lumen area*, mm ²	1.8 (1.2-2.3)	7.4 (1.9-3.0)	<0.001

* Expressed as median and interquartile range.

RWS: radial wall strain; OFR: optical flow ratio; LCR: lipid-to-cap ratio; TCFA, thin-cap fibroatheroma.

Supplementary Table 4. Colocalisation rate of RWS_{max} with maximum LCR.

		RWS_{max} detected segment		
		Proximal segment	Throat segment	Distal segment
Maximum LCR detected segment	Proximal segment	32	9	4
	Throat segment	2	46	5
	Distal segment	4	2	20

LCR, lipid-to-cap ratio; RWS, radial wall strain.

Supplementary Table 5. Diagnostic performance of $RWS_{max} >12\%$ for LCR and TCFA.

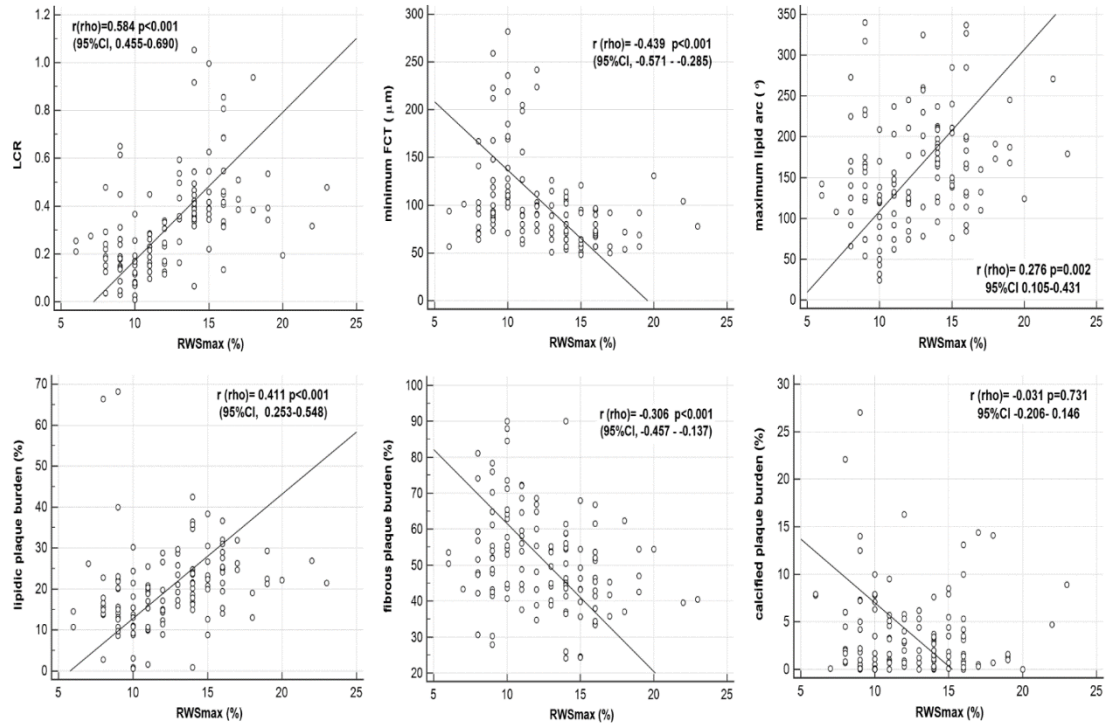
	LCR >0.33 (n=57)	TCFA (+) (n=14)
Sensitivity	86.0	92.9
(95%CI)(%)	(74.2-93.7)	(66.1-99.8)
Specificity	85.1	58.2
(95%CI)(%)	(74.3-92.6)	(48.4-67.5)
PPV	83.1	22.0
(95%CI)(%)	(73.3-89.8)	(17.8-26.9)
NPV	87.7	98.5
(95%CI)(%)	(78.8-93.2)	(90.6-99.8)
+LR	5.8	2.2
(95%CI)	(3.2-10.3)	(1.7-2.9)
-LR	0.2	0.1
(95%CI)	(0.1-0.3)	(0.0-0.8)
Accuracy	85.5	62.1
(95%CI)(%)	(74.2-93.6)	(53.5-71.3)

LCR, lipid-to-cap ratio; RWS, radial wall strain; TCFA, thin-cap fibroatheroma; NPV, negative predictive value; PPV, positive predictive value; +LR, positive likelihood ratio; -LR, negative likelihood ratio.

Supplementary Table 6. Diagnostic performance of $RWS_{max} > 12\%$ for $LCR > 0.33$ in the derivation cohort.

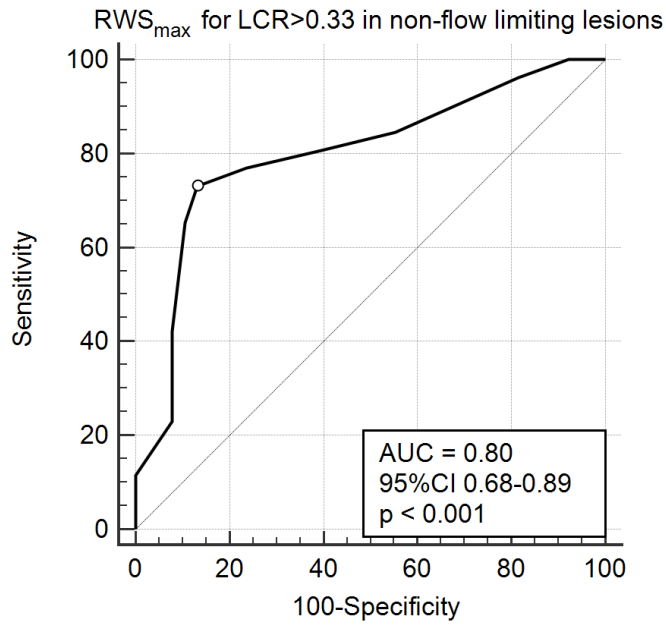
	LCR >0.33 (n=27)
Sensitivity	85.2
(95%CI)(%)	(66.3-95.8)
Specificity	88.6
(95%CI)(%)	(73.3-96.8)
PPV	85.2
(95%CI)(%)	(69.3-93.6)
NPV	88.6
(95%CI)(%)	(75.6-95.1)
+LR	7.5
(95%CI)	(2.9-19.0)
-LR	0.2
(95%CI)	(0.1-0.4)
Accuracy	87.1
(95%CI)(%)	(76.5-95.3)

RWS, radial wall strain; LCR, lipid-to-cap ratio; NPV, negative predictive value; PPV, positive predictive value; +LR, positive likelihood ratio; -LR, negative likelihood ratio



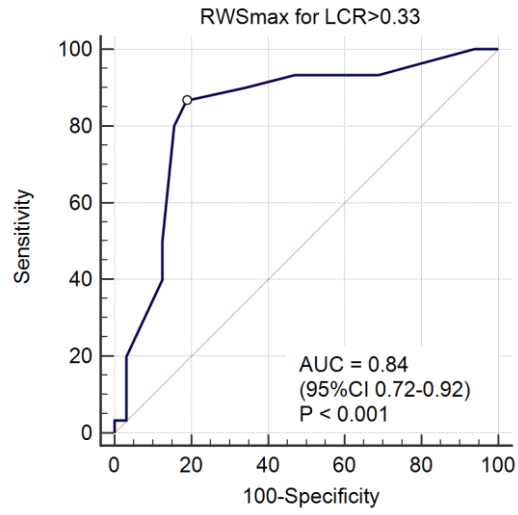
Supplementary Figure 1. Correlation between RWS_{\max} and OCT-derived plaque parameters.

RWS, radial wall strain; OCT, optical coherence tomography; LCR, lipid-to-cap ratio; FCT, fibrous cap thickness.



Supplementary Figure 2. ROC analysis and predictive value of RWS_{max} for LCR >0.33 in non-flow limiting lesions.

RWS, radial wall strain; LCR, lipid-to-cap ratio



Supplementary Figure 3. ROC analysis in the derivation cohort